Supporting Information for Tuning ultrafast electron injection dynamics at organic-graphene/metal interfaces

Abhilash Ravikumar[1], Gregor Kladnik[2,3], Moritz Müller[4], Albano Cossaro[5], Gregor Bavdek[6], Laerte L. Patera[3,5], Daniel Sánchez Portal [4], Latha Venkataraman[7,8], Alberto Morgante[3,5], Gian Paolo Brivio[1], Dean Cvetko[2,5,9] and Guido Fratesi[10]

[1] *Università di Milano-Bicocca,Via Cozzi 55 - 20125 Milano, Italy.*

[2] *Faculty for mathematics and physics, University of Ljubljana, Slovenia*

[3] *Dipartimento di Fisica, Università di Trieste, Italy*

[4] *Centro de Física de Materiales, Paseo Manuel de Lardizabal 5, 20018 San Sebastián, Spain*

[5] *CNR-IOM Laboratorio Nazionale TASC, Trieste, Italy*

[6] *Faculty of education, University of Ljubljana, Ljubljana, Slovenia*

[7] *Dept. of Applied Physics and Applied Mathematics, Columbia University, New York*

[8] *Dept. of Chemistry, Columbia University, New York*

[9] *Institut J. Stefan, Janova 39, Ljubljana, Slovenia*

[10] *Dipartimento di Fisica, Università degli Studi di Milano, Via Celoria, 16 - 20133 Milano, Italy*

---

1 Additional information concerning the simulations

Structural optimization of bipyridine on free-standing graphene

To address the various adsorption configurations of bipyridine on pristine, free-standing graphene (FSG) we extended to this molecule our previous investigation of pyridine and related radicals on graphene[1]. Accordingly, we make use of the ab initio density functional theory (DFT) simulation platform Quantum Espresso [2] that uses pseudopotentials and plane-wave basis set. The system is setup within Generalized Gradient Approximation using Perdew-Burke-Ernzerholf (PBE) ex-

change correlational functional [3, 4] and the Grimme correction is used to take into account non-local van der Waals interaction [5]. Bipyridine is adsorbed on a 5×7 graphene supercell periodic in the *xy* plane and a vacuum separation of 15 Å of periodically repeated systems in the *z* direction. The plane wave kinetic energy cut-off is 42 Ry and the convergence on the energy and force are 10^{-4} a.u. and 10^{-3} a.u., respectively. The surface Brillouin zone is sampled using a 15×14 Γ-centered **k** grid for calculating the system energy and a 18×12 Γ centered grid for the density of states (DOS) calculations (the latter corresponding to a 90×84 grid in the 1×1 unit cell). We considered the configurations shown in Fig. S1, whose energies and structural parameters are summarized in Table 1. The CT-armchair configuration was found to be the most stable, although a mild dependence of the adsorption energy points to high molecular diffusivity and possible coexistence of different adsorption sites. The optimized coordinates of CT-armchair have been chosen as the starting point for the later SIESTA/TranSIESTA structural optimizations and the calculations of the DOS, that instead adopt a localized basis sets (see the main text). We checked the equivalence of the computed DOS of BP/FSG in the ground and excited states by the two approaches.

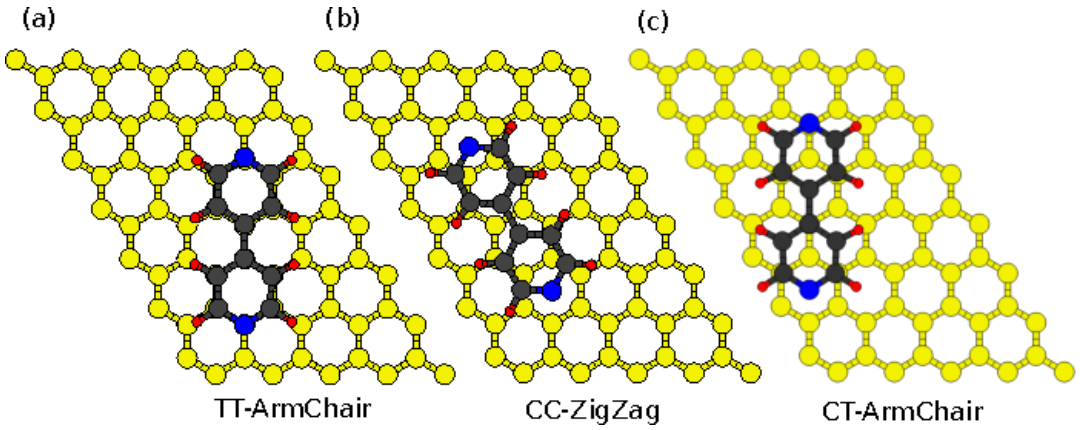

Figure S1: The configurations of bipyridine on graphene which were studied are (a) TT-ArmChair : where the nitrogen atoms of the molecule are on top of the carbon atoms of the graphene ring and the in-plane axis connecting these nitrogen atoms pass above armchair graphene. (b) CC-ZigZag: the nitrogen atoms of the molecule are on the center of a graphene ring with the in-plane axis passing above zigzag graphene. (c) CT-ArmChair: where the nitrogen atoms are on top of a graphene atom and in the center of the graphene ring.

Configuration	E_{ads} (meV)	$a_{BP\text{-}G}$ Å	Torsional angle (θ°)
TT-ArmChair	-679	3.34	9.7
CC-ZigZag	-752	3.23	9.5
CT-ArmChair	-782	3.09	9.2

Table 1: The adsorption energies (E_{ads}), Bipyridine-graphene equilibrium bond distance ($a_{BP\text{-}G}$) and Bipyridine torsional angle (θ) after adsorption is tabulated for these configurations with Grimme correction. Gas phase bipyridine torsional angle is reported to be 37°[6].

Molecular break junction setup

The now describe the break junction setup employed for our calculations of molecules adsorbed on a semi-infinite substrate. We model a semi-infinite substrate to better describe a bulk continuum as shown in Fig. S2. We utilize the Green's function formalism within DFT to deal with such systems. The system is setup as a 6×6 surface supercell with two semi infinite electrode regions and a central scattering one. The electrodes are composed of three Ni layers on either side. The central scattering region consists of bipyridine adsorbed on epitaxial graphene/nickel and bilayer graphene/nickel substrates as shown in Fig. 1(b) and (c) of the main article. With respect to our previous work and in order to reduce the number of atoms involved in the calculation, an asymmetric break-junction setup is used at variance than in our previous calculations [7, 8]. The system is periodic in the *xy* direction and a vacuum separation of 35 Å is used along the transport direction z to ensure minimal interaction between the periodic images and an almost constant electrostatic potential between the asymmetric leads.

The density of states $\rho_\phi(E)$ projected on the molecular orbital ϕ of interest (PDOS) is then fitted by a Lorentzian function to extract the linewidth. Since we are interested in the resonant lifetime for an initially localized state, rather than for one with definite momentum, the evaluation of ρ_ϕ includes an integral over the surface Brillouin zone [7]. However, we could check that in this specific case (LUMO of BP in BP/EG/Ni and BP/BLG/Ni) the contributions to the PDOS at zone center and zone boundary superimpose, so the BZ sampling could be restricted to a coarser mesh (equivalent to a 12×12 one for clean Ni(111)) than for the self-consistent calculations.

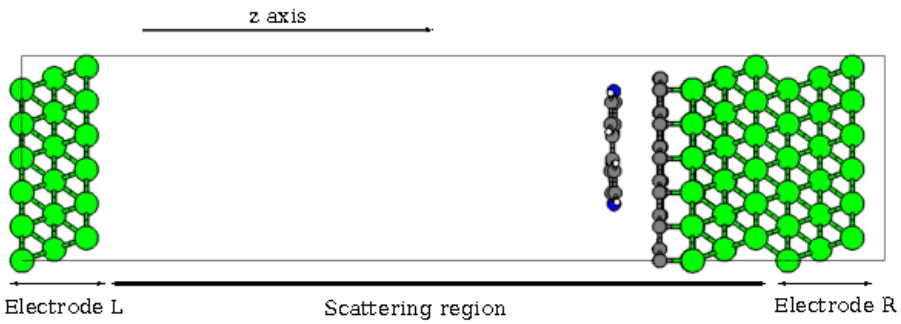

Figure S2: The break junction setup shows three layers of Ni as electrodes on either sides which are coupled to bulk continuum by self energy operators. The central scattering region is asymmetric with the molecule adsorbed on one side and the two regions are decoupled by a large vacuum separation of 35 Å.

Gas phase molecular orbitals of bipyridine

Frontier gas phase molecular orbitals of bipyridine are plotted for reference in Fig. S3. We recall that our analysis focuses on the LUMO so that the relative alignment of the other orbitals (especially of σ with respect to π states, given they suffer differently from self-interaction errors[9]) is not relevant for our results. We mention on this respect that by an additional calculation with an hybrid functional (PBE0)[10] we reproduced the same ordering as reported here.

Density of states for ground state and core-excited adsorbed bipyridine

We report here a detailed decomposition of the DOS for the three systems we have studied.

Figure S4 summarizes the DOS of BP/EG/Ni. The total DOS, and its projections on the top and bottom layers of graphene are shown. Details regarding the DOS are discussed in detail in the main text. We also repeat for convenience the projections onto the molecular orbitals of bipyridine in the ground and core excited state.

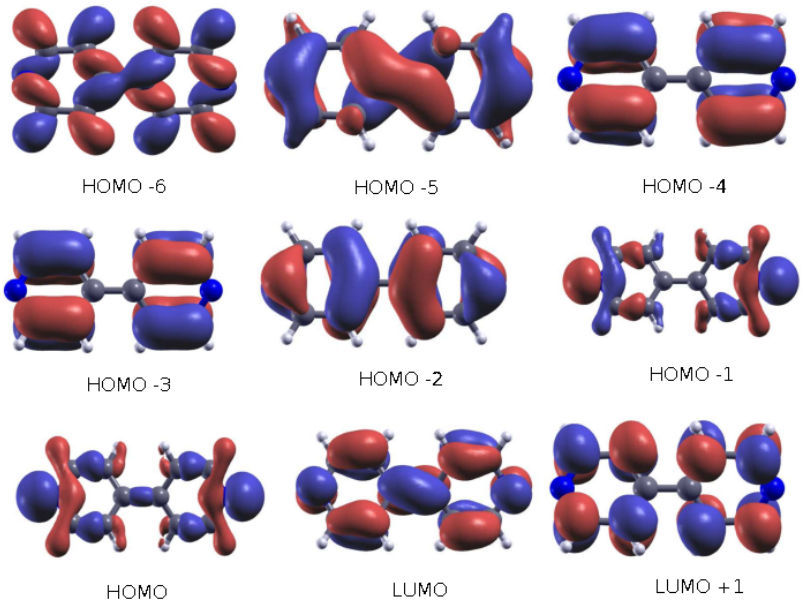

Figure S3: Gas phase molecular orbitals of bipyridine.

Figure S5 summarizes the same quantities for BP/BLG/Ni. Here in addition to the total DOS, its projections on the top and bottom layers of graphene are shown separately.

We also plot the ground and core excited state DOS of BP/FSG as shown in Fig. S6.

Resonant coupling for spin-minority LUMO* states

We now detail the procedure employed to evaluate the charge transfer time for the spin-minority LUMO*. In our spin-collinear electronic structure relaxation, the valence electronic density in the two spin populations is determined self-consistently without any constraint. This resulted in the spin-majority bipyridine state being populated upon the excitation, which represents the electronic ground state (with a N1s atom). In the experiments, resonant core-excitation to the LUMO* state could however equally involve a spin-minority electron. To model this case, that could be though as an inversion of the molecular spin density also given that the electrostatic interaction with the core is the main perturbation to the energy levels of the free molecule, we therefore need to consider a spin-minority LUMO* at about the same energy below the Fermi level, as the spin-majority one

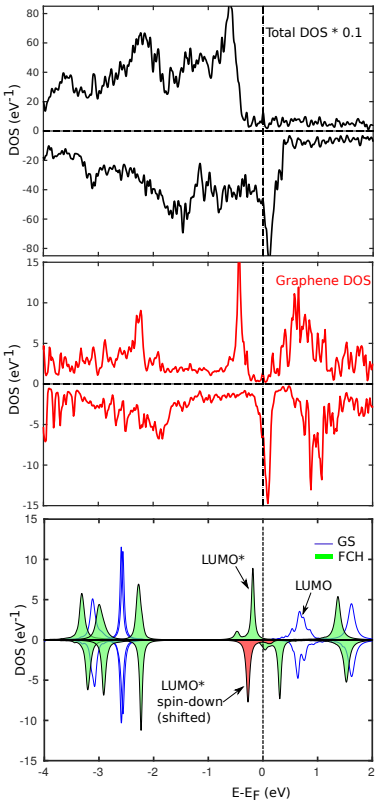

Figure S4: The total DOS of BP/EG/Ni, and its projections on the graphene layer are shown. The projections onto the molecular orbitals in the ground state (GS) and in the core excited one (FCH) are also plotted.

computed self-consistently. This is achieved here by applying as a post-self-consistent correction a shift of the Hamiltonian matrix elements belonging to the molecule, a procedure implemented and tested in our previous work:[7]

$$H_{\mu\nu\mathbf{k}_\parallel} = H_{\mu\nu\mathbf{k}_\parallel} + S_{\mu\nu\mathbf{k}_\parallel}\Delta\varepsilon, \quad \mu,\nu \in \text{molecule}. \tag{1}$$

In the above, S is the overlap operator and $\mu,\nu,\mathbf{k}_\parallel$ stand for the localized basis set indexes and the surface wavevector. By a shift of $\Delta\varepsilon = -0.5$ eV we effectively align the spin-minority LUMO* peak position in the DOS (for example in BP/EG/Ni) to the desired value below the Fermi energy, as shown in Fig. S4 and Fig. S5 for BP/EG/Ni(111) and BP/BLG/Ni(111), respectively. Then we evaluate its resonant fwhm as a result of coupling with spin-minority Ni states.

Work function for EG/Ni(111) and BLG/Ni(111)

The adsorption of graphene on Ni(111) modifies the electrostatic dipole and hence the work function of the substrate, Φ. Our calculations performed for the (1×1) unit cell of EG/Ni(111) (without adsorbed molecules) produced a decrease of Φ by 1.0 eV with respect to the one of clean Ni(111), in agreement to the literature[11] (see Fig. S7). In the case of BLG/Ni(111), Φ is instead reduced by only 0.3 eV, so that the addition of a second layer of graphene over EG/Ni(111) produces an increase of Φ by 0.7 eV. (We notice that an even larger increase of the work function when passing from single to bilayer graphene, 1.0 eV, has been found for a Ru(0001) substrate[12].) This variation is consistent with a similar shift away from the Fermi energy, when passing from BP/EG/Ni to BP/BLG/Ni, that can be appreciated for the BP molecular orbitals in Fig. 2 of the main text.

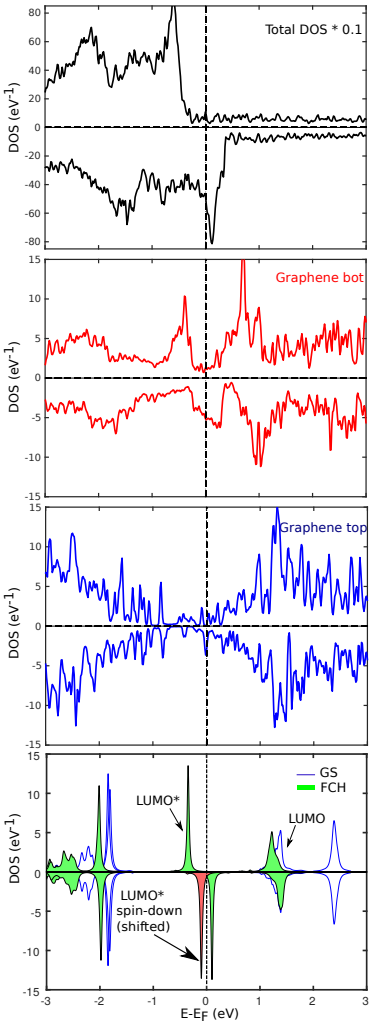

Figure S5: The total DOS of BP/BLG/Ni, and its projections on the bottom and on the top graphene layer are shown. The projections onto the molecular orbitals in the ground state (GS) and in the core excited one (FCH) are also plotted.

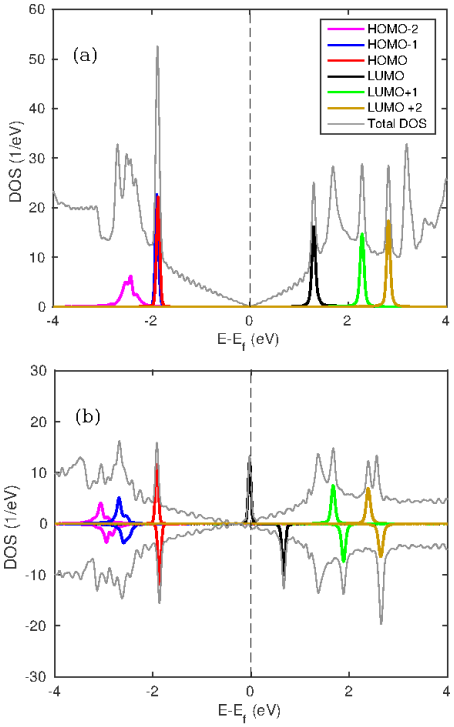

Figure S6: The total DOS of BP/FSG/Ni, its projections onto the molecular orbitals in (a) the ground state and (b) the core excited state are shown.

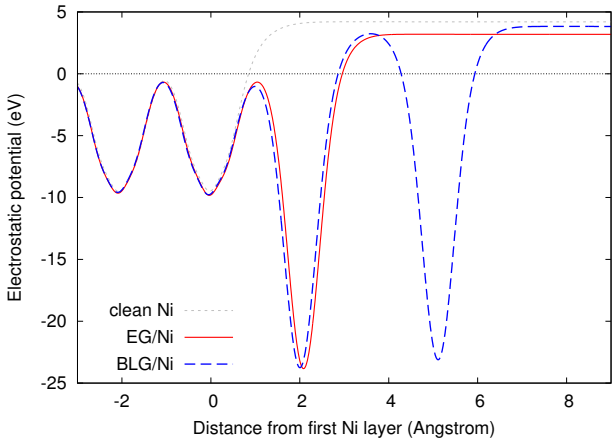

Figure S7: Electrostatic potentials for clean Ni(111), EG/Ni(111), and BLG/Ni(111). Results are averaged over planes parallel to the surface and shown with reference to the Fermi energy.

2 Additional information concerning the experiments

Synthesis of EG and BLG phases of graphene

The synthesis of EG and BLG phases on Ni(111) has been performed in-situ, by ethylene adsorption in 10^{-6} mbar atmosphere on Ni(111) held at 400°C (650°C). The quality of the EG (BLG) phase was monitored by UV photoemission with 40.8 eV photon energy where characteristic π band at Γ at 10.5 eV (8.5 eV) binding energy was evidenced accompanied by adequate attenuation of the Ni3*d* band features, in agreement with preparation procedures reported by Patera et al.[13]. For both phases EG and BLG, carbon 1*s* XPS was regularly checked with characteristic peaks detected at 285 eV (284.5 eV) binding energy.

NEXAFS measurements

Experimental observations of the molecular geometry are studied using Nitrogen 1*s* Near Edge X-ray Absorption Fine Structure (NEXAFS) which is shown in Fig. S8. The NEXAFS for both the systems show a very similar electronic structure the empty bipyridine orbitals. The main peak corresponds to the N1*s* $\rightarrow$LUMO transition. The LUMO of BP has a π character with the nodal plane coinciding with the molecular aromatic ring. The NEXAFS spectra were recorded with photon electric field $\vec{\varepsilon}$ aligned along the substrate normal (p-pol) and with $\vec{\varepsilon}$ lying in the surface plane (s-pol). For BP multilayer the intensity of the LUMO excitation is independent of the electric field polarization, as can be expected for a randomly oriented molecular film. BP/EG/Ni and BP/BLG/Ni monolayer films, on the contrary, display a very strong and almost identical linear dichroism which suggests an almost flat lying adsorption geometry of the molecule. From the π peak intensity analysis we find BP molecular long axis almost parallel to the substrate with average inclination of the BP phenyl rings of 16° and $20° \pm 3°$, for BP/EG/Ni and BP/BLG/Ni, respectively which are in close agreement with theoretically calculated angles.

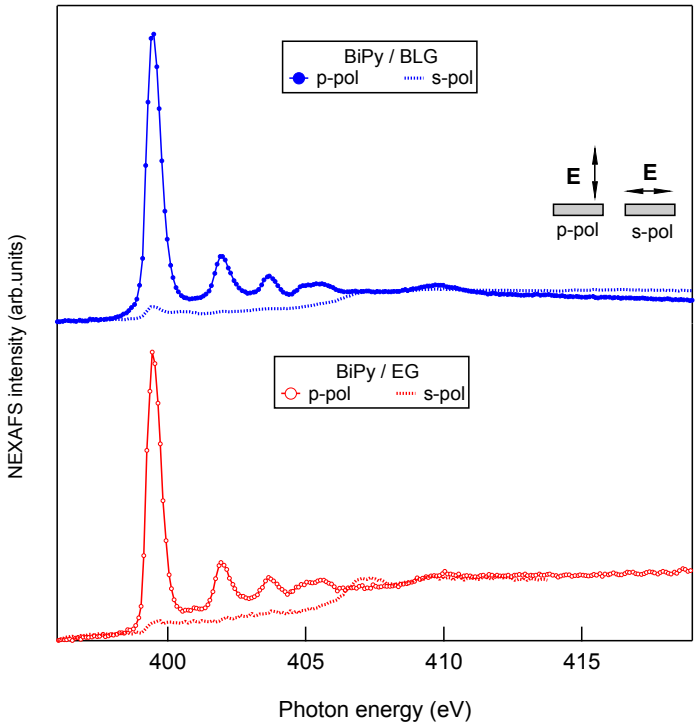

Figure S8: NEXAFS spectra in p-polarization (line with markers) and s-polarization (dashed lines) for BP/EG/Ni (red color, lower panel) and BP/BLG/Ni (blue color, upper panel). The direction of the photon field in the two polarizations is depicted in the inset.

Valence band photoemission

UV valence band photoemission experiments were performed at HASPES /ALOISA beamline with He discharge source using of 40.8 eV from He II line. Angle resolved spectra were collected with a 150 mm hemispherical electron analyzer with 2° acceptance angle, by rotating the sample polar angle in steps of 2° . The overall energy resolution was 0.1 eV. The Ni(111) and EG phase the surface orientation was aligned by rotating sample azimuthal orientation (around surface normal) which allowed us to collect angle resolved spectra along ΓK and ΓM surface directions. For BLG phase there was no azimuthal dependence in the spectra due to polydispersion of azimuthally equivalent domains.

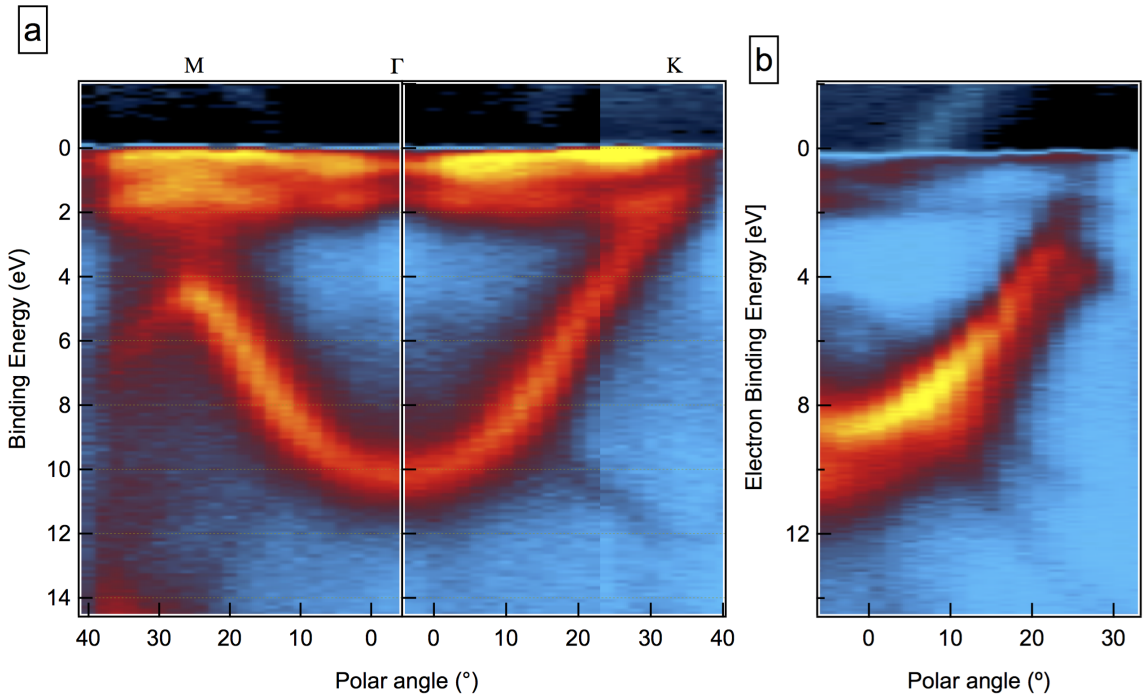

Figure S9: (a) EG phase ARUPS with photon energy of 40.8 eV (He II line) along ΓM and ΓK surface direction, showing the GR π band dispersion with band bottom at Γ reaching −10.5 eV. (b) BLG phase ARUPS with GR band bottom at Γ reaching −8.5 eV, consistent with the electronic structure of poorly interacting topmost GR layer. Some residual of the EG layer beneath may also be observed in the spectrum.

Model for bi-directional electron transfer

In the main text we worked with the assumption that the excited orbital LUMO* lies fully below the Fermi energy. In this section we apply a more elaborate model that we detailed previously[14], which allows for only part of the LUMO* resonance to be aligned below the Fermi level. We recall that in this case charge transfer can be bi-directional: from the substrate to the LUMO*, upon the excitation N1s →free-energy continuum, but also from the LUMO* to the substrate for the on-resonance excitation N1s →LUMO*. Here, two additional variables are introduced leaving with three unknowns: backward/forward transfer times (τ_{BT} and τ_{CT} for the two cases indicated above, respectively) and the fraction of LUMO* aligning below the Fermi energy. By determining the superparticipator/participator intensity ratio in the system of interest (I_{SP}/I_P), and with the

single additional information provided by measuring the uncoupled system (i.e., the multilayer) participator intensity I_P^0, a third condition must be given and we have chosen to fix $\tau_{BT} = \tau_{CT}$. This assumption matches time reversal symmetry of the fundamental process within a model description for the transferred electron, treated as an independent particle on a time-independent potential.

Within this model, Equation (2) in the main text can be used with spectra reported in the main text and repeated in Fig. S10. For BP/EG/Ni, with $I_P/I_P^0 \sim 0.8$ and $I_{SP}/I_P \sim 0.4$, we evaluate a transfer time of $\tau'_{EG} \sim 3.3$ fs similar to the previously reported value of 4 ± 1 fs [15]. For BP/BLG/Ni, having $I_P/I_P^0 \sim 0.8$ also in this case and $I_{SP}/I_P \sim 0.13$ we obtain $\tau'_{BLG} \sim 10$ fs, ~ 3 times slower than for BP/EG/Ni. We remark that the determination of I_P/I_P^0, originating from measurements on different sample, requires further assumptions; our estimate of $I_{SP}/I_P \approx 0.8$ includes a normalization of the intensities by the NEXAFS matrix element for the differently oriented molecules in the multilayer and on graphene.

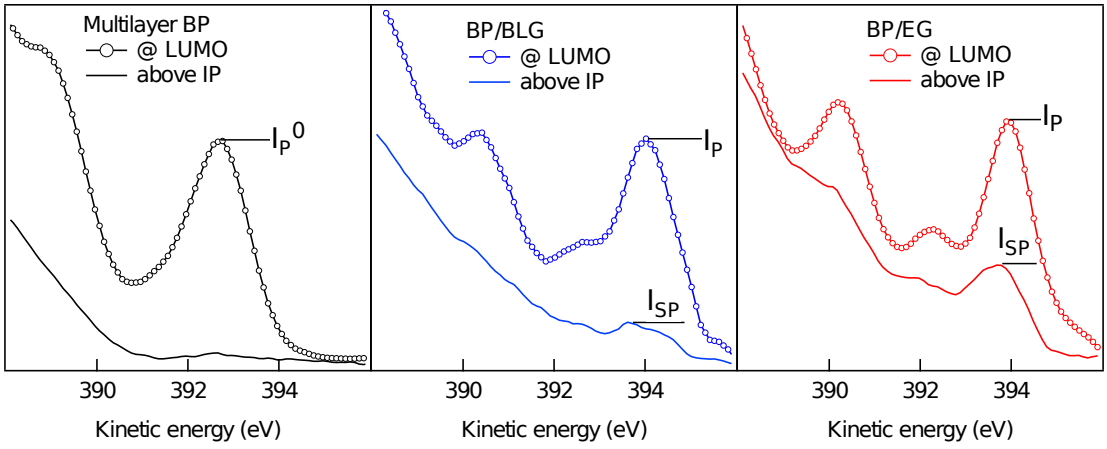

Figure S10: Resonant (on LUMO) and off resonant (above IP) photoemission spectra for BP multilayer (left), monolayer BP/BLG/Ni (middle) and monolayer BP/EG/Ni (right). For charge transfer time analysis we use participator peak (I_P) intensities at N1s $\rightarrow$LUMO* excitation ($E_k = \sim 394$ eV), superparticipator peak (I_{SP}) intensities at N1s $\rightarrow$free electron continuum above IP ($h\nu \sim 404$ eV), and reference participator intensity (I_P^0) from the BP multilayer.

References

[1] A. Ravikumar, A. Baby, H. Lin, G. P. Brivio, and G. Fratesi, "Femtomagnetism in graphene induced by core level excitation of organic adsorbates.," *Scientific reports*, vol. 6, no. April, p. 24603, 2016.

[2] P. Giannozzi, S. Baroni, N. Bonini, M. Calandra, R. Car, C. Cavazzoni, D. Ceresoli, G. L. Chiarotti, M. Cococcioni, I. Dabo, A. Dal Corso, S. de Gironcoli, S. Fabris, G. Fratesi, R. Gebauer, U. Gerstmann, C. Gougoussis, A. Kokalj, M. Lazzeri, L. Martin-Samos, N. Marzari, F. Mauri, R. Mazzarello, S. Paolini, A. Pasquarello, L. Paulatto, C. Sbraccia, S. Scandolo, G. Sclauzero, A. P. Seitsonen, A. Smogunov, P. Umari, and R. M. Wentzcovitch, "QUANTUM ESPRESSO: a modular and open-source software project for quantum simulations of materials.," *Journal of physics. Condensed matter : an Institute of Physics journal*, vol. 21, p. 395502, sep 2009.

[3] J. Perdew, K. Burke, and Y. Wang, "Generalized gradient approximation for the exchange-correlation hole of a many-electron system," *Physical Review B*, vol. 54, pp. 16533–16539, dec 1996.

[4] J. Perdew, K. Burke, and M. Ernzerhof, "Generalized Gradient Approximation Made Simple.," *Physical Review Letters*, vol. 77, pp. 3865–3868, oct 1996.

[5] S. Grimme, "Semiempirical GGA-type density functional constructed with a long-range dispersion correction," *Journal of Computational Chemistry*, vol. 27, pp. 1787–1799, nov 2006.

[6] L. Ould-Moussa, O. Poizat, M. Castella, and M. Curie, "Ab Initio Computations of the Geometrical, Electronic, and Vibrational Properties of the Ground State, the Anion Radical, and the N,N'-Dihydro Cation Radical of 4,4'-Bipyridine Compared to Transient Raman Spectra," *J. Phys. Chem.*, vol. 100, pp. 2072–2082, 1996.

[7] G. Fratesi, C. Motta, M. I. Trioni, G. P. Brivio, and D. Sánchez-Portal, "Resonant Lifetime of Core-Excited Organic Adsorbates from First Principles," *The Journal of Physical Chemistry C*, vol. 118, pp. 8775–8782, may 2014.

[8] D. Cvetko, G. Fratesi, G. Kladnik, A. Cossaro, G. P. Brivio, L. Venkataraman, and A. Morgante, "Ultrafast electron injection into photo-excited organic molecules," *Phys. Chem. Chem. Phys.*, vol. 18, no. 32, pp. 22140–22145, 2016.

[9] S. Refaely-Abramson, S. Sharifzadeh, N. Govind, J. Autschbach, J. B. Neaton, R. Baer, and L. Kronik, "Quasiparticle spectra from a nonempirical optimally tuned range-separated hybrid density functional," *Physical Review Letters*, vol. 109, p. 226405, Nov 2012.

[10] C. Adamo and V. Barone, "Toward reliable density functional methods without adjustable parameters: The pbe0 model," *The Journal of Chemical Physics*, vol. 110, no. 13, p. 6158, 1999.

[11] R. Rosei, S. Modesti, F. Sette, C. Quaresima, A. Savoia, and P. Perfetti, "Electronic structure of carbidic and graphitic carbon on Ni(111)," *Physical Review B*, vol. 29, pp. 3416–3422, Mar. 1984.

[12] P. Sutter, M. S. Hybertsen, J. T. Sadowski, and E. Sutter, "Electronic Structure of Few-Layer Epitaxial Graphene on Ru(0001)," *Nano Letters*, vol. 9, pp. 2654–2660, July 2009.

[13] L. L. Patera, C. Africh, R. S. Weatherup, R. Blume, S. Bhardwaj, C. Castellarin-Cudia, A. Knop-Gericke, R. Schloegl, G. Comelli, S. Hofmann, and C. Cepek, "*In Situ* Observations of the Atomistic Mechanisms of Ni Catalyzed Low Temperature Graphene Growth," *ACS Nano*, vol. 7, pp. 7901–7912, Sept. 2013.

[14] D. Cvetko, G. Fratesi, G. Kladnik, A. Cossaro, G. P. Brivio, L. Venkataraman, and A. Morgante, "Ultrafast electron injection into photo-excited organic molecules," *Phys. Chem. Chem. Phys.*, vol. 18, no. 32, pp. 22140–22145, 2016.

[15] O. Adak, G. Kladnik, G. Bavdek, A. Cossaro, A. Morgante, D. Cvetko, and L. Venkataraman, "Ultrafast Bidirectional Charge Transport and Electron Decoherence at Molecule/Surface Interfaces: A Comparison of Gold, Graphene, and Graphene Nanoribbon Surfaces," *Nano Letters*, vol. 15, no. 12, pp. 8316–8321, 2015.